Cutting-edge spectroscopy techniques highlight toxicity mechanisms of copper oxide nanoparticles in the aquatic plant *Myriophyllum spicatum*

Eva Roubeau Dumont, Arnaud Elger, Céline Azéma, Hiram Castillo Michel, Suzy Surble, Camille Larue

Cutting-edge spectroscopy techniques highlight toxicity mechanisms of copper oxide nanoparticles in the aquatic plant *Myriophyllum spicatum*

Eva Roubeau Dumont[1], Arnaud Elger[1], Céline Azéma[1], Hiram Castillo Michel[2], Suzy Surble[3], Camille Larue[1]

[1]Laboratoire Ecologie Fonctionnelle et Environnement, Université de Toulouse, CNRS, Toulouse, France

[2]Beamline ID21, ESRF-The European Synchrotron, CS40220, 38043, Grenoble Cedex 9, France

[3]Université Paris-Saclay, UMR 3685 CEA/CNRS NIMBE, CEA Saclay 91191, Gif-sur-Yvette, France.

Corresponding author: Camille Larue, camille.larue@ensat.fr

Laboratoire Ecologie Fonctionnelle et Environnement, Campus INPT-ENSAT. Avenue de l'Agrobiopole – BP 32607 - 31326 Castanet Tolosan, France

ABSTRACT

Copper oxide nanoparticles (CuO-NPs) have been increasingly released in aquatic ecosystems over the past decades as they are used in many applications. Cu toxicity to different organisms has already been highlighted in the literature, however toxicity mechanisms of the nanoparticulate form remain unclear. Here, we investigated the effect, transfer and localization of CuO-NPs compared to Cu salt on the aquatic plant *Myriophyllum spicatum*, an ecotoxicological model species with a pivotal role in freshwater ecosystems, to establish a clear mode of action. Plants were exposed to 0.5 mg/L Cu salt, 5 and 70 mg/L CuO-NPs during 96 hours and 10 days. Several morphological and physiological endpoints were measured. Cu salt was found more toxic than CuO-NPs to plants based on all the measured endpoints despite a similar internal Cu concentration demonstrated *via* Cu mapping by micro particle-induced X-ray emission (µPIXE) coupled to Rutherford backscattering spectroscopy (RBS). Biomacromolecule composition investigated by FTIR converged between 70 mg/L CuO-NPs and Cu salt treatments after 10 days. This demonstrates that the difference of toxicity comes from a sudden massive Cu^{2+} addition from Cu salt similar to an acute exposure, versus a progressive leaching of Cu^{2+} from CuO-NPs representing a chronic exposure. Understanding NP toxicity mechanisms can help in the future conception of safer by design NPs and thus diminishing their impact on both the environment and humans.

Keywords: copper, distribution, macrophyte, nanoparticle, toxicity

1. Introduction

The last decades have seen an exponential increase in the use of engineered nanoparticles (NPs), *i.e.* particles with at least one dimension below 100 nm [1]. Their small size confers them properties which are highly valuable for both domestic and industrial purposes, such as in electronics, cosmetics, drug engineering or agriculture [2]. They can be found in many products of our daily life, such as paints, sunscreens, toothpaste and clothing, making them omnipresent in our environment. Products containing NPs increased by 91-fold between 2005 and 2020 [3]. As an example, the global annual production of copper oxide NPs (CuO-NPs) was approximately 570 tons/year in 2014 and is predicted to be 1600 tons/year by 2025 [4]. CuO-NPs are mainly used as biocides [5], [6], and they are included in several applications in agriculture, such as fungicides and herbicides, but also as growth regulators and fertilizers [7]. Such extensive use has led to a direct contamination of many ecosystems whose extent started to be acknowledged by the end of the 2000's in both aquatic and terrestrial environments [8]–[11]. The aquatic environment is known to be especially at risk as it acts as a sink for pollutants

[12]. CuO-NPs are released into aquatic ecosystems through indirect pathways, such as runoffs and leaching from industrial and agricultural sites, and also through direct pathways, with the use of antifouling paints [13], [14], raising a global concern for ecological impacts of such contamination [15].

Negative impacts have been reported on several organisms, although the toxicity range varies depending on the species and environmental factors. Indeed, water quality, organic matter and pH will influence the colloidal stability of metal-based NPs, and thus influence their potential toxicity [16]. It is therefore challenging to assess their effects on aquatic ecosystems. Several studies have been performed on aquatic species to assess the mode of action and toxicity of CuO-NPs and if it stems from ionic leaching or particle-specific toxicity. No consensus has been reached so far. Especially, the mechanisms behind toxicity in aquatic plants remain unclear. Few studies found that aquatic plant species were more sensitive to the nanoparticulate form than the ionic one [17]–[21], while another study on duckweed attributed toxicity to ionic leaching from CuO-NPs [22]. Finally, one study performed on a submerged rooted aquatic plant species, *Elodea nuttaliii*, showed similar effects between Cu salt and CuO-NP exposure on growth and down-regulation of a Cu transporter gene, COPT1, after 24h of exposure [23], suggesting that toxicity was due to ionic leaching. In order to understand better the toxicity mechanisms, we need to access Cu spatial distribution which is not investigated in most studies. For this purpose, biophysical techniques represent a great asset even though they are not often used in environmental sciences. Indeed, spectroscopic techniques have proven to be effective tools to assess metal uptake and distribution in organisms at high spatial resolution [24]. The combination of micro particle-induced X-ray emission (µPIXE) with Rutherford backscattering spectroscopy (RBS) provides unique *in situ* information on elemental mapping in plant tissues and is highly relevant to assess uptake of metal based NPs [25].

In this study, we aimed at making use of cutting-edge spectroscopic techniques to bring new and original data to answer the question of the mechanisms of action implied in CuO-NP toxicity in aquatic plants in comparison with Cu salt. *Myriophyllum spicatum* (L.), a submerged OECD model species (OECD TG 238, 239), was used to link dissolution, adsorption, absorption, and Cu localization to CuO-NP mode of action. Cu distribution was analysed using µPIXE coupled to RBS to avoid mixing the Cu signal coming from Cu adsorbed at the surface of leaves with Cu really absorbed inside the leaf tissues, allowing to map Cu distribution in leaf cross-sections. Additionally, Cu toxicity was assessed through "traditional" biomarkers (such as growth, dry matter content and photosystem efficiency) and by evaluating its impact on plant biomacromolecule composition via Fourier-transformed infrared spectroscopy (FTIR) analysis.

2. Material and methods

2.1. Plant growth and Cu exposure

M. spicatum L. (Haloragaceae) was chosen as a model species of aquatic freshwater species (see supporting information for more details about plant growth). In total, two concentrations of CuO-NPs were used: 5 and 70 mg/L; along with one control concentration (0 mg/L) and one $CuSO_4$ concentration containing 0.5 mg/L Cu^{2+}, with n = 10 per concentration (see supporting information for more details about exposure protocol) for either 96h or 10 days of exposure. CuO-NP concentrations were chosen based on literature and preliminary experiments allowing proper Cu visualization inside leaf tissues by µPIXE/RBS. Although no information on environmental CuO-NP concentration can be found, studies have highlighted Cu^{2+} concentrations up to 100 mg/kg in European topsoils [26] and Cu concentration of 40 mg/kg in freshwater sediments are considered environmentally-relevant [27], [28].

2.2. Nanoparticle characterization

The nominal diameter of NPs was determined using Transmission Electron Microscopy (TEM, Jem-1400, Jeol, USA), and imageJ software for image analysis (n = 45). Nanoparticle hydrodynamic diameter in suspension was assessed by dynamic light scattering (DLS; Zetasizer Nano ZS90, Malvern Panalytical, UK) and the software Zetasizer (n = 3). The zeta potential in plant culture medium was measured with 12 runs for both suspensions (Zetasizer Nano ZS90, Malvern Panalytical, UK). Nanoparticle dissolution at the end of exposure in plant exposure medium was assessed by ICP-OES (see supplementary materials for more details).

2.3. Copper leaching and concentration in plant samples

Copper concentrations in the media were measured by sampling water at the beginning and at the end of exposure from experimental units of both Cu exposure times (96 h and 10 days) in order to assess effective concentrations. Copper concentration in plants was measured at the end of Cu exposure after acid digestion of dry plant material. For more details about sample preparation see supporting information.

Copper and other elemental (Ca, K, P, Fe, S, Mg, Mo, Mn, Zn) concentrations in both plants and media were measured using ICP-OES (Iris Intrepid II XLD, Thermo Electron, MA, USA) with a detection limit of 0.0012 mg/kg for water samples and 0.00169 mg/kg for plant samples. Different controls were analysed to ensure the quality of the measurements.

2.4. Exposure endpoints

2.4.1. Growth-related endpoints

Fresh mass was measured at the beginning and at the end of exposure after having gently dried the plants with blotting paper, to calculate the relative growth rate based on biomass production (RGR). Samples were oven-dried at 70 °C during 72 h before weighting again to measure their dry matter content (DMC).

RGR was calculated for each experimental unit as follows:

$$RGR_{i-j} = (\ln(Nj) - \ln(Ni)) \,/\, t$$

where RGR_{i-j} is the relative growth rate from time i to j, N_i and N_j is the endpoint (fresh mass) in the test or control vessel at time i and j, respectively, and t is the time period in days from i to j.

DMC in % was calculated as:

$$\%DMC = \left(\frac{100 \times DM}{FM}\right)$$

where FM is the fresh mass of a plant sample, DM is its corresponding dry mass.

2.4.2. Physiological endpoints

Oxidative stress was evaluated through lipid peroxidation measurements, using the production of malondialdehyde (MDA) in the samples to assess membrane integrity according to Parveen et al. (2017) [29] (more details in supporting information).

Quantum efficiency of photosystem II was estimated at the end of exposure for each experimental unit using the Fv/Fm ratio, which is the ratio of the variable (Fv) to the maximum chlorophyll fluorescence (Fm), *i.e*. the maximal ability of the plant to harvest light [30]. Measurements were conducted using a

Diving-PAM fluorometer (Heinz Walz GmbH, Germany) in a dark chamber, 30 min after dark acclimatization of the plant to ensure that all reaction centers were opened for new photons. The basic settings of the Diving-PAM, namely intensity of measuring light (50: MEAS-INT) and amplification factor (49: GAIN) were set to 8 and 2, respectively.

2.4.3. Biomacromolecule composition

Biomacromolecule composition was determined by Fourier transformed infrared spectroscopy (FTIR). Plant samples were dried for 48 h at 105°C, then ground in thin powder (> 20 mg). Samples were analysed using a FTIR microscope in attenuated total reflection (ATR) mode (Thermo Nicolet NEXUS 470 ESR, ThermoFisher™, Massachusetts, USA) over the frequency range of 4000 – 400 cm^{-1} with a spectral resolution of 4 cm^{-1}. One spectrum was an average of 64 scans per sample. Each powdered plant was placed on the sample plate and three independent technical replicates for each sample (10 biological replicates per treatment) were acquired. OMNIC software was used to export experimental spectra after ATR correction (OMNIC™ FTIR Software, ThermoFisher™, Massachusetts, USA). FTIR data treatment was performed using Orange software [31]. Briefly, data were pre-processed which implies selection of the region of interest (including most of the variance among samples), vector normalization and smoothing by Savitzky-Golay filter. Using the second derivative, a principal component analysis (PCA) was carried out for the different exposure times (n=30 per time of exposure × condition with technical replicates). The components permitting to explain at least 70% of the variance were used to perform a subsequent linear discriminant analysis (LDA). This approach permitted to plot the samples and detect differences among groups of samples. When a difference was detected, a logistic regression was applied to the pre-processed data to identify wavenumbers contributing to the difference detected among groups by the PCLDA.

2.4.4. Spatial distribution and semi-quantification of Cu

Absorption and adsorption of Cu in leaves were mapped and measured using a nuclear microprobe. A combination of micro-particle induced X-ray emission (µPIXE) and Rutherford backscattered spectroscopy (RBS) was used for elemental mapping and semi-quantification. Leaves were thoroughly washed three times with deionized water to take off Cu lightly bound to the surface and immersed in a droplet of resin (Tissue Teck Sakura®) to be immediately cryo-fixed by plunging the sample in isopentane cooled with liquid nitrogen. Samples were then cut in thin cross-sections (40 µm) using a cryo-microtome (Leica, Germany) and finally freeze-dried (48 h, -52°C, 0.01 mbar). Freeze-dried sections were analyzed at the nuclear microprobe available at the Atomic Energy Commission (CEA) Center of Saclay (France) with a proton source of 3 MeV, a beam focused to 2.5 µm and a current intensity of 500 pA. Data processing was performed using Rismin software [32] to define regions of interest and extract spectra, and SIMNRA [33] and GUPIX [34] codes to fit RBS and PIXE data, respectively. The Cu/(K+Ca) ratio was used as a Cu enrichment indicator as K and Ca are the most abundant endogenous elements.

2.4.5. Statistical analyses

Results were analyzed using the R studio software (R Core Team (2016) V 3.3.1) and analyses were performed within each exposure time (96 h and 10 days). Homoscedasticity was tested using Bartlett test. Data normality was assessed with Shapiro-Wilk test on ANOVA residuals, with log-transformation when normality assumption was not met. Two-way ANOVAs were performed on results showing normal distribution, with or without log transformation, to assess the interactive effects of Cu concentrations and time of exposure. Tukey HSD post-hoc tests were used to identify significant differences among Cu concentrations and exposure times. Kruskal-Wallis tests were used in dataset when no normality was found despite log-transformation. The differences in plant inorganic composition resulting from exposure were assessed using a linear discriminant analysis (LDA, n = 10, ade4 package [35]). The significance of the discriminant analyses was assessed using Monte-Carlo tests with 1000 repetitions.

3. Results

3.1. CuO-NP characterization, Cu^{2+} concentration and leaching

Nominal diameter of CuO-NPs was on average 64.9 ± 8.5 nm according to TEM images (n = 45, **Fig. 1A**). Sedimentation was visually observed with NP deposition on the leaves of *M. spicatum* after the first 2 hours of exposure, forming a thin black layer (**Fig. S1**). Hydrodynamic diameter measured at different times showed agglomeration of NPs from the beginning of exposure with no strong evolution over time, except after 10 days at the highest concentration (**Fig. 1B**). Hydrodynamic diameter based on Z-average was 331 nm after 96 h of exposure for both concentrations, and 59 nm and 321 nm after 10 days of exposure at 5 mg/L and 70 mg/L CuO-NPs, respectively. Finally, the zeta potential of CuO-NPs in Smart & Barko was -21.7 ± 3.5 mV.

Total Cu in the medium for all concentrations at the beginning of exposure were 0, 0.48 ± 0.01 mg/L for $CuSO_4$, 4.44 ± 0.61 mg/L and 70.22 ± 4.73 mg/L for CuO-NPs. Cu^{2+} concentration in $CuSO_4$ treatment was 0.14 ± 0.05 mg/L after 96 h and 0.17 ± 0.03 mg/L after 10 days of exposure. Regarding CuO-NP treatments, a small proportion of Cu^{2+} leached over time from the NPs, with 11.5 % and 0.8 % of Cu^{2+} from 5 and 70 mg/L CuO-NP suspensions measured in the water column after 96 h, respectively (2-way ANOVA, $F_{1,20}$ = 1178.2, P < 0.0001, **Fig. 1C**). After 96h, the leached Cu^{2+} concentrations from NPs in the water column corresponded to the Cu salt treatment with final Cu^{2+}

concentration in the medium of 0.5 mg/L. After 10 days of exposure, the Cu^{2+} concentration in the medium decreased by 86% and 79% for 5 mg/L and 70 mg/L CuO-NP suspensions, respectively, likely due to NP sedimentation on sediment (**Fig. S1**) and to plant adsorption/absorption of Cu^{2+}.

3.2. Copper concentration and distribution in plants

Significant differences in bulk Cu concentrations in plants were observed among treatments (2-way ANOVA, $F_{3,72} = 3784.903$, $P < 0.0001$) but not between times of exposure. On average at both exposure times, Cu concentrations in plants were 4.7 ± 0.5, 8.1 ± 1.1 and 41.7 ± 4.7 mg/g dry weight (DW) of plants exposed to 0.5 mg/L Cu salt, 5 and 70 mg/L CuO-NPs, respectively (**Fig. 2A**).

To go further into Cu internalization and localization in plant leaf, spatial distribution analysis was performed on plants exposed to 0, 0.5 mg/L Cu salt and 70 mg/L CuO-NPs for 10 days. Homeostasis level of Cu was found in control plants for basal metabolism (**Fig. 2B, C**), whereas significantly higher accumulation of Cu was found at 0.5 mg/L Cu salt (**Fig. 2D**) and 70 mg/L CuO-NPs (**Fig. 2E,** 2-way ANOVA, $F_{2,38} = 340.64$, $P < 0.0001$). The highest Cu accumulation was detected on leaf epidermis for both treatments, with more than 3 times Cu level in plant sections exposed to 70 mg/L CuO-NPs compared to plants exposed to 0.5 mg/L Cu salt (**Fig. 2E**). Cu accumulation decreased in parenchyma and vascular cylinder and was similar for both treatments. Our results showed that Cu from both treatments was internalized by the plants in parenchyma and vascular tissues.

3.3. Copper toxicity to plants

3.3.1. Copper toxicity based on “traditional” endpoints

Relative growth rate was only significantly impacted by Cu salt exposure, inhibiting growth by 57% after 96 h and by 80% after 10 days of exposure (2-way ANOVA, $F_{3,72}$ = 12.64, P < 0.0001, **Fig. 3A**). CuO-NP exposure inhibited growth by 30% at 70 mg/L after 10 days of exposure, however the variation among replicates was too high to highlight a significant difference.

Dry matter content significantly increased after 10 days of exposure at 0.5 mg/L Cu salt, with 14% of DMC in exposed plants against 8% for others (2-way ANOVA, $F_{3,71}$ = 6.423 P = 0.0149, **Fig. 3B**).

Lipid peroxidation levels were significantly increased at both exposure times for 0.5 mg/L Cu salt, and after 10 days of exposure to 70 mg/L CuO-NPs (2-way ANOVA, $F_{3,63}$ = 21.559, P < 0.001, **Fig. 3C**). An interactive effect was found between treatments and exposure time (2-way ANOVA, $F_{3,63}$ = 5.333, P = 0.002), with a significant effect of CuO-NPs on lipid peroxidation only after 10d of exposure compared to Cu salt.

Finally, no significant effect of CuO-NPs was observed on Fv/Fm at any concentration despite the deposition of a thin black layer on plant leaves, whereas Cu salt significantly decreased Fv/Fm by 12% after 96 h of exposure (2-way ANOVA, $F_{3,72}$ =12.956, P < 0.001, **Fig. S1 & S2**).

3.3.2. Copper toxicity based on biomacromolecule composition

Biomacromolecule composition significantly changed among treatments at both exposure times (**Fig. 4**). The significant differences and the peak interpretations are listed in **Table 1**. After 96 h of exposure, plants at 0.5 mg/L Cu salt segregated from other treatments based on the first and third dimensions of the PCA toward the up-right corner, and plants exposed to 70 mg/L CuO-NPs segregated along the first dimension on the right side (**Fig. 4A, B**). Plants exposed to Cu segregated from the control based on the first dimension, with an overlap between 5 and 70 mg/L CuO-NPs treatments. These differences in composition were observed mostly in proteins, phenolic compounds, carbohydrates and cellulosic compounds (**Table 1**). After 10 days of exposure, plants exposed to 5 mg/L CuO-NPs remained the closest to control plants in terms of composition and remained on the left side of the first dimension, whereas composition from plants exposed at 0.5 mg/L Cu salt and 70 mg/L CuO-NPs converged on the right side of the same dimension (**Fig. 4C, D**). The plants exposed to these two treatments exhibited higher absorbances for the peaks representing polysaccharides, carbohydrates and proteins compared to control plants (**Table 1**).

3.3.3 Effect of Cu exposure on plant ionome

Plant exposure to ionic Cu and CuO-NPs significantly influenced their inorganic composition after 96 h and 10 days, as revealed by the linear discriminant analyses (LDA) based on ICP-OES measurements realized on the whole plants (Monte-Carlo test, P = 0.001, 22.47 % and 22.62% of inertia explained, respectively, **Fig S3**). A significant increase of Ca concentrations was observed at both times of exposures for plants exposed to ionic Cu (2-way ANOVA, $F_{3,72} = 40.41$, $P < 0.001$), whereas plants exposed to 70 mg/L CuO-NPs showed a significantly higher Ca concentration only after 96 h (**Fig. S4A**). Magnesium concentration significantly increased in plants exposed to ionic Cu after 96 h, and increased both in ionic Cu and 70 mg/L CuO-NPs treatments after 10 days (Kruskal-Wallis, df = 3, $P < 0.001$, **Fig. S4B**). Sulfur concentration in plants significantly decreased after 10 d of exposure to ionic Cu (2-way ANOVA, $F_{2,50} = 5.61$, $P < 0.001$, **Fig. S4C**) whereas Zn concentration was significantly higher for plants exposed to 70 mg/L CuO-NPs at both times of exposure (Kruskal-wallis, df = 3, $P < 0.005$, **Fig. S4D**).

These results were similar to those found by µPIXE/RBS in plant leaves after 10 days (**Fig. S5**). Calcium concentrations were significantly higher for plants exposed to ionic Cu, and found rather accumulated in parenchyma and epidermis tissues (**Fig. S5A**). Sulfur was found significantly more abundant in plants exposed to CuO-NPs with no difference in distribution among tissues due to variation among cross-sections (**Fig. S5B**) and Zn was found at higher concentrations in plants exposed to CuO-NPs at 70 mg/L, with no difference in distribution among plant tissues (**Fig. S5C**).

4. DISCUSSION

Our results, based on an original combination of spectroscopic techniques (FTIR and µPIXE/RBS) and a thorough characterization of NP dynamics in suspension, suggest that Cu ion leaching is the main driver of CuO-NP toxicity even though a specific nano form effect cannot be excluded but would remain minor. These conclusions confirmed some data available in the literature on different organisms. Indeed, few studies suggest that the most prominent mode of action of CuO-NPs on organisms is the leaching of ionic Cu^{2+} from NPs, inducing reactive oxygen species (ROS) production and subsequent stress in organisms [15], [36]. This is shared by most heavy-metal based NPs which are prone to dissolution, such as Ag-NPs or ZnO-NPs [5], [37]–[39], although some NPs, such as TiO_2 and CeO_2, behave differently [40], [41]. This mode of action was shown from single-cell organisms [42]–[44], to more complex organisms such as zooplankton, fish and aquatic plant species [45]–[47]. A big difference in toxicity can be found from one study to another in the literature even within a same species, which may be related to environmental conditions [15], [18].

Indeed, the behavior of NPs and the subsequent ionic leaching is directly linked to water physico-chemical parameters [47]. In our exposure conditions, CuO-NPs were prone to quickly form agglomerates as a result of low repulsive forces, high surface energy and high ionic strength of the medium leading to a high sedimentation rate, as demonstrated by the NP deposition on leaves. The same kind of results was obtained in the literature for other heavy-metal based NPs [48]–[50]. The presence of $CaCl_2$ in the Smart & Barko medium likely increased the formation of agglomerates and sedimentation speed, as Ca^{2+} is known to form bridges in solution [51]. The black deposition on the plant leaves visually observed suggests that CuO-NPs were tightly adsorbed at the plant surface as it was not eliminated with several washing steps. Shi *et al.* (2013) noticed a similar black deposition on the roots of *Elsholtzia splendens*, a terrestrial plant, after hydroponic exposure which resulted in very high concentrations at the surface of plant roots [49].

The Cu^{2+} concentration **leached** from CuO-NPs after 96 h was similar between the two CuO-NP treatments and equivalent to the Cu salt concentration in solution (*i.e.* 0.5 mg/L). After 10 days of exposure, Cu^{2+} leached from CuO-NPs was still similar between the two concentrations, but strongly decreased compared to the concentration found at 96 h. This could be explained by the continuous uptake of Cu^{2+} by plants, leading to Cu decrease in the water column. Furthermore, underwater photosynthesis changes the pH over time through the release of HCO_3^-, which can influence colloidal stability and increase the formation of agglomerates, decreasing ionic leaching [52], [53]. This, combined with the formation of hetero-agglomerates with organic matter produced by *M. spicatum*, can decrease further the colloidal stability and ionic leaching, as it is proportional to the surface area to volume ratio [49], [51], [53]–[55].

In our study, CuO-NPs were less toxic to *M. spicatum* than Cu salt, especially after 96 h where no effect of NPs was observed, whereas Cu^{2+} concentration in the medium was similar between Cu salt and NPs. An increase in lipid peroxidation was observed after 10 days of exposure to 70 mg/L CuO-NPs and was the only significant sign of toxicity when copper was provided under a NP form. On the other hand, Cu salt strongly decreased growth and increased lipid peroxidation at both exposure times, and increased DMC after 10 days as a result of stress [56], [57]. This result could be surprising as Cu bulk concentration was higher (by a factor of 9) in plants exposed to 70 mg/L CuO-NPs compared to plants exposed to Cu salts.

However, Cu bulk concentration does not give any information as to Cu internalization and localization, especially as CuO-NP accumulation was visible on plant surface. The data provided by the µPIXE/RBS analysis confirmed that Cu mostly accumulated on the plant surface (epidermis) with a factor of 3 between Cu salts and CuO-NPs 70 mg/L, even if this difference was not significant due to high variation among replicates. Furthermore, when focusing on the internalized Cu, a similar concentration was found in plants exposed to Cu salt and to 70 mg/L CuO-NPs. This is also in line with the fact that equivalent ionic Cu concentrations were measured in the medium suggesting an internalization which is mainly occurring under ionic form. Previous work has shown that ionic internalization is detected through an homogenous distribution with µPIXE, whereas a dot-like distribution is linked to nanoparticulate form [24]. In our study, internalization of NPs themselves cannot be excluded as some highly concentrated sub-micrometric to micrometric spots were detected by µPIXE inside leaf parenchyma, compared to the more homogeneous Cu distribution in the vascular tissues. This phenomenon has also been demonstrated in other studies on both terrestrial and aquatic species [18], [21], [58], [59], but further investigations using X-ray absorption spectroscopy would be needed for speciation confirmation. Indeed, some studies demonstrated that aquatic species, such as *Chlorella pyrenoidosa* and *Eichhornia crassipes,* were able to transform CuO-NPs into other Cu species, such as Cu_2S or Cu_2O-NPs, highlighting the need to go deeper into the speciation of CuO-NP once it enters biological barriers as speciation can influence both its translocation and toxicity [18], [60].

These findings explain why such a high Cu concentration in plants exposed to CuO-NPs was found by ICP, but do not explain why Cu salt was more toxic to the plants despite a similar internal concentration found by µPIXE/RBS. This difference in toxicity between Cu salt and CuO-NP treatments can be explained by the sudden addition of soluble Cu salt compared to the progressive leaching of ionic Cu from CuO-NPs [61]. The results for biomacromolecule composition support these findings as a gradual convergence between plants exposed to 70 mg/L CuO-NPs and Cu salt was observed during exposure. A strong effect of Cu salt was observed on plant composition after 96 h compared to CuO-NP treatments (5 and 70 mg/L) whereas the overall ionic Cu concentration in the medium was similar. This lower impact of NPs despite similar ionic concentration as Cu salt suggests that the leaching was progressive, and the subsequent stress was of lower amplitude and mitigated over the duration of our exposure. A change in phenolic compounds, proteins and cellulosic compounds was observed in plants exposed to Cu salts, likely as the result of a stress, and possibly corresponding to an antioxidant response [45], [62], [63], as well as a mechanism to maintain membrane integrity [59], [64]. Additionally, ICP-OES and µPIXE/RBS analyses showed changes in concentrations of S or Zn mostly impacted by ionic Cu and by CuO-NPs to a smaller extent. It could be linked to shifts in the antioxidant balance, as these elements act as co-factors for several detoxification enzymes and Cu regulation pathways [65]–[67]. An interesting response was the increased Ca concentration and its distribution primarily in epidermis tissues. Studies have shown that Ca was an important part of the signaling pathway and stress response in plants, for instance with the calmodulin pathways for signaling or the formation of egg box structures for heavy metal regulation in cell walls [66], [68]. More specific assays would be necessary to assess the extent of the stress response triggered by exposure, and its specific pathways, by targeting mechanisms such as enzymatic activities, transcription, and production of antioxidant compounds.

Several studies on different aquatic micro and macro-organisms have found similar results in which Cu internal concentration resulting from CuO-NP exposure was not correlated to the observed toxicity, and the ionic counterpart was much more toxic for a similar or lower internal concentration, supporting our finding [17], [23], [42], [61], [69]. For instance Wu *et al*. (2020) demonstrated no correlation between toxicity and Cu concentration in three aquatic organisms exposed to CuO-NPs, compared to Cu salt [15]. Adam *et al.* (2015) found a higher toxicity in *Daphnia magna* exposed to Cu salt whereas Cu concentration was higher in organisms exposed to CuO-NPs. The toxicity of CuO-NPs was attributed to the Cu ions formed during NP dissolution [70]. Similarly, the marine bacteria *Vibrio anguillarum* showed a lower sensitivity to CuO-NPs than to Cu salt, and toxic effects were attributed to progressive Cu ions leaching from NPs [43].

Overall, exposure to Cu salt can be considered as an acute exposure to ionic Cu, triggering a rapid and strong change in plant physiology, whereas exposure to CuO-NPs corresponds to a chronic exposure to ionic Cu, inducing progressive physiological adjustments of lower amplitude. The antioxidant balance can mitigate a chronic exposure over time by inducing progressive physiological changes [62], [64], whereas an acute exposure could lead to a tipping point where the stress can no longer be copped with [23], [71].

5. CONCLUSION

This study assessed the toxicity of CuO-NPs compared to Cu ions from $CuSO_4$ salt on *M. spicatum*, a model aquatic plant species. Based on our observations, the toxicity of CuO-NPs appeared driven by a progressive ionic leaching from NPs and was found less toxic than Cu salt, as the plant was able to adapt and mitigate stress over time through physiological changes. Cutting-edge techniques showed that most of the Cu leached from NPs was adsorbed at the plant leaf surface rather than absorbed, which would have not been possible with other bulk analyses such as ICP-OES. µPIXE/RBS provided a new perception of the links between toxicity and accumulation regarding heavy metal-based NPs. Thanks to high-throughput FTIR technique, we were able to visualize global biomacromolecule composition shifts resulting from exposure. In future experiments, we will investigate more specific response patterns such as phenolic compound production and cell walls components. These findings do not exclude a nanospecific toxicity mechanism, as NP internalization was suggested by µPIXE, but further studies on speciation within organisms remain to be done.

ACKNOWLEDGMENTS

This research was funded by the French Ministry of research and higher education through a Doctoral Fellowship awarded to Dr Eva Roubeau Dumont. We thank Emmanuel Flahaut and Vincent Baylac from the CIRIMAT, Toulouse, for their contribution on NP characterization regarding the trainings on Turbiscan and DLS measurements, Lucas Vigier for his implication in methodological developments of MDA protocols and Clarisse Liné for the TEM pictures. Authors have no competing interest to declare.

Author's contribution: **ERD**: Conceptualization, Investigation, Data acquisition, Data Curation, Formal analysis, Writing - Original draft preparation, **AE**: Writing – original draft preparation, Funding Acquisition, Supervision, **CA**: Data acquisition, **SS**: Resources, Data acquisition, Data analysis, **HCM:** Resources, Data acquisition, **CL**: Conceptualization, Data acquisition, Data analysis, Writing-Original draft preparation, Supervision.

REFERENCES

[1] D. R. Boverhof *et al.*, “Comparative assessment of nanomaterial definitions and safety evaluation considerations,” *Regul. Toxicol. Pharmacol.*, vol. 73, no. 1, pp. 137–150, 2015, doi: 10.1016/j.yrtph.2015.06.001.

[2] M. Bundschuh *et al.*, “Nanoparticles in the environment: where do we come from, where do we go to?,” *Environ. Sci. Eur.*, vol. 30, no. 1, 2018, doi: 10.1186/s12302-018-0132-6.

[3] D. Environment, “Search Database - The Nanodatabase.” [Online]. Available: https://nanodb.dk/en/search-database/. [Accessed: 18-Nov-2020].

[4] A. A. Keller, S. McFerran, A. Lazareva, and S. Suh, “Global life cycle releases of engineered nanomaterials,” *J. Nanoparticle Res.*, vol. 15, no. 6, 2013, doi: 10.1007/s11051-013-1692-4.

[5] A. Ivask *et al.*, “Mechanisms of toxic action of Ag, ZnO and CuO nanoparticles to selected ecotoxicological test organisms and mammalian cells in vitro : A comparative review,” *Nanotoxicology*, vol. 8, no. sup1, pp. 57–71, Aug. 2014, doi: 10.3109/17435390.2013.855831.

[6] L. A. Tamayo *et al.*, “Release of silver and copper nanoparticles from polyethylene nanocomposites and their penetration into Listeria monocytogenes,” *Mater. Sci. Eng. C*, vol. 40, pp. 24–31, 2014, doi: 10.1016/j.msec.2014.03.037.

[7] T. Xiong *et al.*, “Copper Oxide Nanoparticle Foliar Uptake, Phytotoxicity, and Consequences for Sustainable Urban Agriculture,” *Environ. Sci. Technol.*, vol. 51, no. 9, pp. 5242–5251, 2017, doi: 10.1021/acs.est.6b05546.

[8] W.-M. Lee, Y.-J. An, H. Yoon, and H.-S. Kweon, “Toxicity and bioavailability of copper nanoparticles to the terrestrial plants mung bean (phaseolus radiatus) and wheat (*triticum aestivum*): plant agar test for water-insoluble nanoparticles,” *Environ. Toxicol. Chem.*, vol. 27, no. 9, p. 1915, 2008, doi: 10.1897/07-481.1.

[9] V. Shah and I. Belozerova, “Influence of metal nanoparticles on the soil microbial community and germination of lettuce seeds,” *Water. Air. Soil Pollut.*, vol. 197, no. 1–4, pp. 143–148, 2009, doi: 10.1007/s11270-008-9797-6.

[10] D. H. Atha *et al.*, “Copper oxide nanoparticle mediated DNA damage in terrestrial plant models,” *Environ. Sci. Technol.*, vol. 46, no. 3, pp. 1819–1827, 2012, doi: 10.1021/es202660k.

[11] C. O. Dimkpa, D. E. Latta, J. E. McLean, D. W. Britt, M. I. Boyanov, and A. J. Anderson, “Fate of CuO and ZnO nano- and microparticles in the plant environment,” *Environ. Sci. Technol.*, vol. 47, no. 9, pp. 4734–4742, 2013, doi: 10.1021/es304736y.

[12] I. Bashir, F. A. Lone, R. A. Bhat, S. A. Mir, Z. A. Dar, and S. A. Dar, “Concerns and Threats of Contamination on Aquatic Ecosystems,” *Bioremediation Biotechnol.*, pp. 1–26, 2020, doi: 10.1007/978-3-030-35691-0_1.

[13] A. S. Adeleye, E. A. Oranu, M. Tao, and A. A. Keller, “Release and detection of nanosized copper from a commercial antifouling paint,” *Water Res.*, vol. 102, pp. 374–382, 2016, doi: 10.1016/j.watres.2016.06.056.

[14] C. Muller-Karanassos, W. Arundel, P. K. Lindeque, T. Vance, A. Turner, and M. Cole,

"Environmental concentrations of antifouling paint particles are toxic to sediment-dwelling invertebrates," *Environ. Pollut.*, vol. 268, p. 115754, 2020, doi: 10.1016/j.envpol.2020.115754.

[15] F. Wu, B. J. Harper, L. E. Crandon, and S. L. Harper, "Assessment of Cu and CuO nanoparticle ecological responses using laboratory small-scale microcosms," *Environ. Sci. Nano*, vol. 7, no. 1, pp. 105–115, 2020, doi: 10.1039/c9en01026b.

[16] C. Peng *et al.*, "Transformation of CuO nanoparticles in the aquatic environment: Influence of pH, electrolytes and natural organic matter," *Nanomaterials*, vol. 7, no. 10, 2017, doi: 10.3390/nano7100326.

[17] G. Song *et al.*, "Effects of CuO nanoparticles on *Lemna minor*," *Bot. Stud.*, vol. 57, no. 1, p. 3, Dec. 2016, doi: 10.1186/s40529-016-0118-x.

[18] J. Zhao *et al.*, "Uptake, Distribution, and Transformation of CuO NPs in a Floating Plant *Eichhornia crassipes* and Related Stomatal Responses," *Environ. Sci. Technol.*, vol. 51, no. 13, pp. 7686–7695, 2017, doi: 10.1021/acs.est.7b01602.

[19] J. Dolenc Koce, "Effects of exposure to nano and bulk sized TiO2 and CuO in Lemna minor," *Plant Physiol. Biochem.*, vol. 119, pp. 43–49, 2017, doi: 10.1016/j.plaphy.2017.08.014.

[20] J. Shi, A. D. Abid, I. M. Kennedy, K. R. Hristova, and W. K. Silk, "To duckweeds (*Landoltia punctata*), nanoparticulate copper oxide is more inhibitory than the soluble copper in the bulk solution," *Environ. Pollut.*, vol. 159, no. 5, pp. 1277–1282, 2011, doi: 10.1016/j.envpol.2011.01.028.

[21] D. Zhang *et al.*, "Uptake and accumulation of CuO nanoparticles and CdS/ZnS quantum dot nanoparticles by Schoenoplectus tabernaemontani in hydroponic mesocosms," *Ecol. Eng.*, vol. 70, pp. 114–123, 2014, doi: 10.1016/j.ecoleng.2014.04.018.

[22] F. Perreault, M. Samadani, and D. Dewez, "Effect of soluble copper released from copper oxide nanoparticles solubilisation on growth and photosynthetic processes of Lemna gibba L," *Nanotoxicology*, vol. 8, no. 4, pp. 374–382, 2014, doi: 10.3109/17435390.2013.789936.

[23] N. Regier, C. Cosio, N. von Moos, and V. I. Slaveykova, "Effects of copper-oxide nanoparticles, dissolved copper and ultraviolet radiation on copper bioaccumulation, photosynthesis and oxidative stress in the aquatic macrophyte *Elodea nuttallii*," *Chemosphere*, vol. 128, pp. 56–61, 2015, doi: 10.1016/j.chemosphere.2014.12.078.

[24] C. Larue *et al.*, "Innovative combination of spectroscopic techniques to reveal nanoparticle fate in a crop plant," *Spectrochim. Acta - Part B At. Spectrosc.*, vol. 119, pp. 17–24, 2016, doi: 10.1016/j.sab.2016.03.005.

[25] H. A. Castillo-Michel, C. Larue, A. E. Pradas del Real, M. Cotte, and G. Sarret, "Practical review on the use of synchrotron based micro- and nano- X-ray fluorescence mapping and X-ray absorption spectroscopy to investigate the interactions between plants and engineered nanomaterials," *Plant Physiol. Biochem.*, vol. 110, pp. 13–32, 2017, doi: 10.1016/j.plaphy.2016.07.018.

[26] C. Ballabio *et al.*, "Copper distribution in European topsoils: An assessment based on LUCAS soil survey," *Sci. Total Environ.*, vol. 636, no. April, pp. 282–298, 2018, doi: https://doi.org/10.1016/j.scitotenv.2018.04.268.

[27] A. M. Ahmed, E. Lyautey, C. Bonnineau, A. Dabrin, and S. Pesce, “Environmental concentrations of copper, alone or in mixture with arsenic, can impact river sediment microbial community structure and functions,” *Front. Microbiol.*, vol. 9, no. AUG, pp. 1–13, 2018, doi: 10.3389/fmicb.2018.01852.

[28] K. J. Rader, R. F. Carbonaro, E. D. van Hullebusch, S. Baken, and K. Delbeke, “The Fate of Copper Added to Surface Water: Field, Laboratory, and Modeling Studies,” *Environ. Toxicol. Chem.*, vol. 38, no. 7, pp. 1386–1399, 2019, doi: 10.1002/etc.4440.

[29] M. Parveen, T. Asaeda, and M. H. Rashid, “Biochemical adaptations of four submerged macrophytes under combined exposure to hypoxia and hydrogen sulphide,” *PLoS One*, vol. 12, no. 8, pp. 1–12, 2017, doi: 10.1371/journal.pone.0182691.

[30] E. H. Murchie and T. Lawson, “Chlorophyll fluorescence analysis: A guide to good practice and understanding some new applications,” *J. Exp. Bot.*, vol. 64, no. 13, pp. 3983–3998, 2013, doi: 10.1093/jxb/ert208.

[31] J. Demšar *et al.*, “Orange: Data mining toolbox in Python,” *J. Mach. Learn. Res.*, vol. 14, p. 23492353, 2013.

[32] L. Daudin, H. Khodja, and J. P. Gallien, “Development of ‘position-charge-time’ tagged spectrometry for ion beam microanalysis,” *Nucl. Instruments Methods Phys. Res. Sect. B Beam Interact. with Mater. Atoms*, vol. 210, pp. 153–158, 2003, doi: 10.1016/S0168-583X(03)01008-5.

[33] M. Mayer, “SIMNRA, a simulation program for the analysis of NRA, RBS and ERDA,” *AIP Conf. Proc.*, no. 541, pp. 514–544, 2008, doi: https://doi.org/10.1063/1.59188.

[34] J. L. Campbell, T. L. Hopman, J. A. Maxwell, and Z. Nejedly, “Guelph PIXE software package III: alternative proton database,” *Nucl. Instruments Methods Phys. Res. Sect. B Beam Interact. with Mater. Atoms*, vol. 170, no. 1, pp. 193–204, 2000, doi: 10.1016/S0168-583X(00)00156-7.

[35] S. Dray and a B. Dufour, “Package ‘ade4,’” *J. Stat. Sorftware*, vol. 22, pp. 1–20, 2007, doi: 10.18637/jss.v022.i04>.License.

[36] N. Malhotra, T. R. Ger, B. Uapipatanakul, J. C. Huang, K. H. C. Chen, and C. Der Hsiao, “Review of copper and copper nanoparticle toxicity in fish,” *Nanomaterials*, vol. 10, no. 6, pp. 1–28, 2020, doi: 10.3390/nano10061126.

[37] V. Aruoja, H. C. Dubourguier, K. Kasemets, and A. Kahru, “Toxicity of nanoparticles of CuO, ZnO and TiO2 to microalgae Pseudokirchneriella subcapitata,” *Sci. Total Environ.*, vol. 407, no. 4, pp. 1461–1468, 2009, doi: 10.1016/j.scitotenv.2008.10.053.

[38] J. Y. Roh, H. J. Eom, and J. Choi, “Involvement of caenohabditis elegans mapk signaling pathways in oxidative stress response induced by silver nanoparticles exposure,” *Toxicol. Res.*, vol. 28, no. 1, pp. 19–24, 2012, doi: 10.5487/TR.2012.28.1.019.

[39] S. K. Kahlon, G. Sharma, J. M. Julka, A. Kumar, S. Sharma, and F. J. Stadler, “Impact of heavy metals and nanoparticles on aquatic biota,” *Environ. Chem. Lett.*, vol. 16, no. 3, pp. 919–946, 2018, doi: 10.1007/s10311-018-0737-4.

[40] J. Hou *et al.*, “Toxicity and mechanisms of action of titanium dioxide nanoparticles in living

organisms," *J. Environ. Sci. (China)*, vol. 75, no. Shiguo Li, pp. 40–53, 2019, doi: 10.1016/j.jes.2018.06.010.

[41] A. Bour *et al.*, "Toxicity of CeO2 nanoparticles at different trophic levels - Effects on diatoms, chironomids and amphibians," *Chemosphere*, vol. 120, pp. 230–236, 2015, doi: 10.1016/j.chemosphere.2014.07.012.

[42] C. Gunawan, W. Y. Teoh, C. P. Marquis, and R. Amal, "Cytotoxic Origin of Copper (II) Oxide Nanoparticles : Comparative Studies and Metal Salts," *AcsNano*, vol. 5, no. 9, pp. 7214–7225, 2011.

[43] A. Rotini *et al.*, "Salinity-based toxicity of CuO nanoparticles, CuO-bulk and Cu ion to vibrio anguillarum," *Front. Microbiol.*, vol. 8, no. OCT, 2017, doi: 10.3389/fmicb.2017.02076.

[44] D. Wang *et al.*, "Where does the toxicity of metal oxide nanoparticles come from: The nanoparticles, the ions, or a combination of both?," *J. Hazard. Mater.*, vol. 308, pp. 328–334, May 2016, doi: 10.1016/j.jhazmat.2016.01.066.

[45] L. Yue, J. Zhao, X. Yu, K. Lv, Z. Wang, and B. Xing, "Interaction of CuO nanoparticles with duckweed (Lemna minor. L): Uptake, distribution and ROS production sites," *Environ. Pollut.*, vol. 243, pp. 543–552, 2018, doi: 10.1016/j.envpol.2018.09.013.

[46] M. J. Baek, J. Son, J. Park, Y. Seol, B. Sung, and Y. J. Kim, "Quantitative prediction of mixture toxicity of AgNO3 and ZnO nanoparticles on Daphnia magna," *Sci. Technol. Adv. Mater.*, vol. 21, no. 1, pp. 333–345, 2020, doi: 10.1080/14686996.2020.1766343.

[47] M. Ozmen, A. Gungordu, and H. Geckil, "Ecotoxicity of Nanomaterials in Aquatic Environment," in *Nanotechnology for Food, Agriculture, and Environment*, D. Thangadurai, J. Sangeetha, and R. Prasad, Eds. Cham: Springer International Publishing, 2020, pp. 351–377.

[48] R. Khan, M. A. Inam, S. Z. Zam, M. Akram, S. Shin, and I. T. Yeom, "Coagulation and dissolution of CuO nanoparticles in the presence of dissolved organic matter under different pH values," *Sustainability*, vol. 11, no. 10, 2019, doi: 10.3390/su11102825.

[49] J. Shi *et al.*, "Phytotoxicity and accumulation of copper oxide nanoparticles to the Cu-tolerant plant Elsholtzia splendens," *Nanotoxicology*, vol. 8, no. 2, pp. 179–188, 2013, doi: 10.3109/17435390.2013.766768.

[50] U. Song and S. Lee, "Phytotoxicity and accumulation of zinc oxide nanoparticles on the aquatic plants Hydrilla verticillata and Phragmites Australis: leaf-type-dependent responses," *Environ. Sci. Pollut. Res.*, 2016, doi: 10.1007/s11356-015-5982-5.

[51] V. S. Sousa and M. R. Teixeira, "Aggregation kinetics and surface charge of CuO nanoparticles: The influence of pH, ionic strength and humic acids," *Environ. Chem.*, vol. 10, no. 4, pp. 313–322, 2013, doi: 10.1071/EN13001.

[52] O. Pedersen, T. D. Colmer, and K. Sand-Jensen, "Underwater photosynthesis of submerged plants - recent advances and methods," *Front. Plant Sci.*, vol. 4, no. May, p. 140, 2013, doi: 10.3389/fpls.2013.00140.

[53] Y. Qiu, Z. Mu, N. Wang, X. Wang, M. Xu, and H. Li, "The aggregation and sedimentation of two different sized copper oxide nanoparticles in soil solutions: Dependence on pH and

dissolved organic matter," *Sci. Total Environ.*, vol. 731, p. 139215, 2020, doi: 10.1016/j.scitotenv.2020.139215.

[54] J. Leitner, D. Sedmidubský, and O. Jankovský, "Size and shape-dependent solubility of CuO nanostructures," *Materials (Basel).*, vol. 12, no. 20, pp. 1–10, 2019, doi: 10.3390/ma12203355.

[55] E. M. Gross, H. Meyer, and G. Schilling, "Release and ecological impact of algicidal hydrolysable polyphenols in *Myriophyllum spicatum*," *Phytochemistry*, vol. 41, no. 1, pp. 133–138, 1996, doi: 10.1016/0031-9422(95)00598-6.

[56] A. Michalak, "Phenolic compounds and their antioxidant activity in plants growing under heavy metal stress," *Polish J. Environ. Stud.*, vol. 15, no. 4, pp. 523–530, 2006.

[57] A. Elger and N. J. Willby, "Leaf dry matter content as an integrative expression of plant palatability: the case of freshwater macrophytes," *Funct. Ecol.*, vol. 17, no. 1, pp. 58–65, Feb. 2003, doi: 10.1046/j.1365-2435.2003.00700.x.

[58] J. Yuan, A. He, S. Huang, J. Hua, and G. D. Sheng, "Internalization and Phytotoxic Effects of CuO Nanoparticles in Arabidopsis thaliana as Revealed by Fatty Acid Profiles," *Environ. Sci. Technol.*, vol. 50, no. 19, pp. 10437–10447, 2016, doi: 10.1021/acs.est.6b02613.

[59] Y. Dai *et al.*, "Interaction of CuO nanoparticles with plant cells: Internalization, oxidative stress, electron transport chain disruption, and toxicogenomic responses," *Environ. Sci. Nano*, vol. 5, no. 10, pp. 2269–2281, 2018, doi: 10.1039/c8en00222c.

[60] J. Zhao *et al.*, "Interactions of CuO nanoparticles with the algae Chlorella pyrenoidosa: adhesion, uptake, and toxicity," *Nanotoxicology*, vol. 10, no. 9, pp. 1297–1305, 2016, doi: 10.1080/17435390.2016.1206149.

[61] F. Perreault, M. Samadani, and D. Dewez, "Effect of soluble copper released from copper oxide nanoparticles solubilisation on growth and photosynthetic processes of *Lemna gibba* L," *Nanotoxicology*, pp. 1–9, 2013, doi: 10.3109/17435390.2013.789936.

[62] M. Hasanuzzaman *et al.*, "Reactive oxygen species and antioxidant defense in plants under abiotic stress: Revisiting the crucial role of a universal defense regulator," *Antioxidants*, vol. 9, no. 8, pp. 1–52, 2020, doi: 10.3390/antiox9080681.

[63] A. Sivaci, E. R. Sivaci, and M. Sökmen, "Changes in antioxidant activity, total phenolic and abscisic acid constituents in the aquatic plants *Myriophyllum spicatum* L. and *Myriophyllum triphyllum* Orchard exposed to cadmium," *Ecotoxicology*, vol. 16, no. 5, pp. 423–428, 2007, doi: 10.1007/s10646-007-0145-1.

[64] X. Wang, H. Zheng, J. Zhao, X. Luo, Z. Wang, and B. Xing, "Photodegradation Elevated the Toxicity of Polystyrene Microplastics to Grouper (Epinephelus moara) through Disrupting Hepatic Lipid Homeostasis," *Environ. Sci. Technol.*, vol. 54, no. 10, pp. 6202–6212, 2020, doi: 10.1021/acs.est.9b07016.

[65] G. Han *et al.*, "C2H2 Zinc Finger Proteins: Master Regulators of Abiotic Stress Responses in Plants," *Front. Plant Sci.*, vol. 11, no. February, pp. 1–13, 2020, doi: 10.3389/fpls.2020.00115.

[66] S. K. Jalmi *et al.*, "Traversing the links between heavy metal stress and plant signaling," *Front. Plant Sci.*, vol. 9, no. February, pp. 1–21, 2018, doi: 10.3389/fpls.2018.00012.

[67] M. A. Hossain, P. Piyatida, J. A. T. da Silva, and M. Fujita, “Molecular Mechanism of Heavy Metal Toxicity and Tolerance in Plants: Central Role of Glutathione in Detoxification of Reactive Oxygen Species and Methylglyoxal and in Heavy Metal Chelation,” *J. Bot.*, vol. 2012, no. Cd, pp. 1–37, 2012, doi: 10.1155/2012/872875.

[68] I. V. Kosakivska, L. M. Babenko, K. O. Romanenko, I. Y. Korotka, and G. Potters, “Molecular mechanisms of plant adaptive responses to heavy metals stress,” *Cell Biol. Int.*, vol. 45, no. 2, pp. 258–272, 2021, doi: 10.1002/cbin.11503.

[69] F. Arratia, P. Olivares-Ferretti, A. García-Rodríguez, R. Marcos, and E. R. Carmona, “Comparative toxic effects of copper-based nanoparticles and their microparticles in Daphnia magna by using natural freshwater media,” *New Zeal. J. Mar. Freshw. Res.*, vol. 53, no. 3, pp. 460–469, 2019, doi: 10.1080/00288330.2019.1598447.

[70] N. Adam, A. Vakurov, D. Knapen, and R. Blust, “The chronic toxicity of CuO nanoparticles and copper salt to *Daphnia magna*,” *J. Hazard. Mater.*, vol. 283, pp. 416–422, 2015, doi: 10.1016/j.jhazmat.2014.09.037.

[71] A. A. Keller *et al.*, “Comparative environmental fate and toxicity of copper nanomaterials,” *NanoImpact*, vol. 7, no. March, pp. 28–40, 2017, doi: 10.1016/j.impact.2017.05.003.

[72] M. Regvar, D. Eichert, B. Kaulich, A. Gianoncelli, P. Pongrac, and K. Vogel-Mikuš, “Biochemical characterization of cell types within leaves of metal-hyperaccumulating *Noccaea praecox* (Brassicaceae),” *Plant Soil*, vol. 373, no. 1–2, pp. 157–171, 2013, doi: 10.1007/s11104-013-1768-z.

[73] H. E. Tahir *et al.*, “Rapid prediction of phenolic compounds and antioxidant activity of Sudanese honey using Raman and Fourier transform infrared (FT-IR) spectroscopy,” *Food Chem.*, vol. 226, pp. 202–211, 2017, doi: 10.1016/j.foodchem.2017.01.024.

[74] S. T. Gorgulu, M. Dogan, and F. Severcan, “2007 Society for Applied Spectroscopy sevgi türker görgülü.pdf,” vol. 61, no. 3, pp. 300–308, 2007.

[75] P. Rajiv, A. Deepa, P. Vanathi, and D. Vidhya, “Screening for Phytochemicals and Ftir Analysis of Myristica Dactyloids Fruit Extracts,” *Int. J. Pharm. Pharm. Sci.*, vol. 9, no. 1, p. 315, 2016, doi: 10.22159/ijpps.2017v9i1.11053.

[76] R. M. B. O. Duarte, C. A. Pio, and A. C. Duarte, “Spectroscopic study of the water-soluble organic matter isolated from atmospheric aerosols collected under different atmospheric conditions,” *Anal. Chim. Acta*, vol. 530, no. 1, pp. 7–14, 2005, doi: 10.1016/j.aca.2004.08.049.

[77] D. T. Bonetta, M. Facette, T. K. Raab, and C. R. Somerville, “Genetic dissection of plant cell-wall biosynthesis.,” *Biochem. Soc. Trans.*, vol. 30, no. 2, pp. 298–301, Apr. 2002, doi: 10.1042/.

[78] N. Abidi, L. Cabrales, and E. Hequet, “Fourier transform infrared spectroscopic approach to the study of the secondary cell wall development in cotton fiber,” *Cellulose*, vol. 17, no. 2, pp. 309–320, 2010, doi: 10.1007/s10570-009-9366-1.

[79] X. Qu *et al.*, “Quantitative and qualitative characteristics of dissolved organic matter from eight dominant aquatic macrophytes in Lake Dianchi, China,” *Environ. Sci. Pollut. Res.*, vol. 20, no. 10, pp. 7413–7423, 2013, doi: 10.1007/s11356-013-1761-3.

[80] K. Arun, K. Pingal, and S. T. Somasundaram, “Phenolic composition , Antioxidant activity and FT-IR Spectroscopic Analysis of *Halophyte Sesuvium portulacastrum* L . extract,” *Int. Res. J. Biol. Sci.*, vol. 5, no. 1, pp. 1–13, 2016.

[81] M. Ibrahim, O. Osman, A. A. Mahmoud, and H. Elhaes, “Spectroscopic analyses of water hyacinth: FTIR and modeling approaches,” *Der Pharma Chem.*, vol. 7, no. 9, pp. 182–188, 2015.

[82] M. S. Pontes *et al.*, “In vitro and in vivo impact assessment of eco-designed CuO nanoparticles on non-target aquatic photoautotrophic organisms,” *J. Hazard. Mater.*, vol. 396, no. February, p. 122484, 2020, doi: 10.1016/j.jhazmat.2020.122484.

Table 1. Spectral assignment and significant differences in biomacromolecule composition of *M. spicatum* exposed to Cu salt at 0.5 mg/L and CuO-NPs at 5 and 70 mg/L during 96 hours and 10 days. Peak numbers refer to Figure 4, the significant differences are either between (-) concentrations, or one treatment differs from all others (alone). Significant differences were set at p-value < 0.05 and were calculated with ANOVAs on Orange software for each wavenumber.

	Peaks	**Significant differences**	**Wavenumber cm^{-1}**	**Definition of the spectral assignment**
	1	0.5	1630-1610	C=O stretching carbonyl, C=C aromatic ring vibration [72] related to phenolic compounds [73]
	2	0 - 0.5, 70	1580-1570	C=N and N-H stretching from proteins [74]
	3	0 - 0.5, 70	1482-1470	C-H bending, structural carbohydrate [75]
	4	0 - 0.5, 70	1390-1380	C-H bending vibrations [76]
96h	5	0.5	1210-1180	C-O stretching from alcohol, esters, amide III from proteins, from polysaccharides in cellulosic compounds [77]
	6	0 – 5, 70	1065	S=O stretching from sulfoxides [72], C-O stretching from polysaccharides [74]
	7	0 - 0.5, 70	1017	C-O stretch from carbohydrates [75], [78]
	8	0 - 70	1000-985	C=C bending from alkene, C-O stretching from polysaccharides [79]
	9	0.5	940-900	C=O, C=C bending from alkene [80]
	1	0.5	1735-1705	C=O stretching, esters from lipids, polysaccharides from cellulose [74], [81] and phenolic compounds [73]
	2	0	1574	C=N and N-H stretching from proteins [74]
	3	5 - 0	1502	C=C aromatic stretching bond [76]
	4	0, 5 - 0.5, 70	1430-1370	C-H bending vibrations [76]
10d	5	0	1320	C-O, C-H and C-N stretching vibration in polysaccharides, aromatic amines and cellulosic compounds [75], [82]
	6	0	1200-1175	C-O stretching from polysaccharides in cellulosic compounds [75], [77]
	7	0, 5, 70 – 0, 5	1140-1125	C-O stretching from carbohydrates [75]
	8	0 - 0.5	1098	C-C and C-O stretches in carbohydrate [73]
	9	0 - 70	1037-1004	OH and C-OH stretching from cell wall polysaccharides [74]

Figure captions

Figure 1. (**A**) Nominal diameter of CuO-NPs through Transmission Electron Microscope, (**B**) NP hydrodynamic diameter in Smart and Barko medium (**C**) Ionic Cu^{2+} leached from CuO-NP suspensions of 5 and 70 mg/L after 96 hours and 10 days. Different lowercase letters represent significant differences among experimental conditions (HSD Tukey test after 2-way ANOVA), *n* = 6.

Figure 2. (**A**) Cu concentrations in *Myriophyllum spicatum* plants measured with ICP-OES *n* = 10 and (**B**, **C**, **D**, **E**) distribution of Cu analysed by micro-particle induced X-ray emission coupled to Rutherford backscattered spectroscopy in leaf cross-section. (**B**) displays semi quantitative information (Cu/(K+Ca)) in the different tissues of the cross-section (all: data for the full section, ep: epidermis, par: parenchyma, vc: vascular cylinder). Lowercase letters indicate significant differences among conditions according to HSD-Tukey test following 2-way ANOVA ($p<0.05$) ± SE, *n* = 4. Maps show without (**C**) or with Cu contamination: 0.5 mg/L Cu salt (**D**) or 70 mg/L CuO nanoparticles (**E**) for 10 days. Scale bar: 20 µm. Color scale in the third map of CuO-NPs condition has been set to the same level than the Cu map of the Cu salt condition for easier comparison.

Figure 3. (**A**) Relative growth rates with Cu^{2+} leached from CuO-NPs in mg/L displayed in italic, (**B**) Dry matter content in % and (**C**) Malondialdehyde in nmol/g fresh weight of *M. spicatum* exposed to 0, 0.5 mg/L Cu^{2+} from $CuSO_4$, 5 and 70 mg/L CuO-NPs for 96 hours or 10 days. 2-way ANOVA P-values for Cu effects are provided; similar lowercase letters indicate conditions that did not significantly differ (HSD Tukey test), ± SE, *n* = 10 except for MDA where *n* = 6.

Figure 4. Biomacromolecule composition of *M. spicatum* analyzed by FTIR exposed to Cu salt at 0.5 mg/L and CuO-NPs at 5 and 70 mg/L during (**A**) 96 hours and (**C**) 10 days with significant differences among treatments highlighted by a logistic regression marked with black arrows (n=120 per exposure time), and PCLDA analyses of the FTIR spectra for exposures during (**B**) 96 hours and (**D**) 10 days. Numbers in **A**, **C** refers to the peaks listed in Table 1.

Figure 1

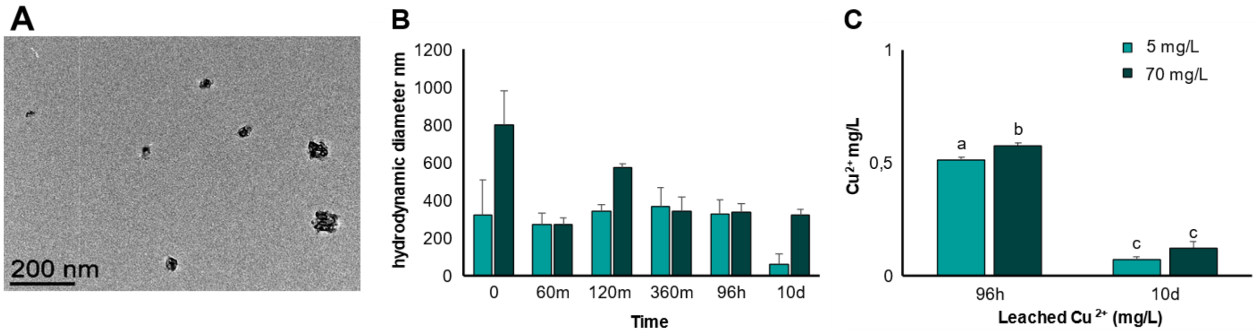
A
200 nm
B
hydrodynamic diameter nm
1200
1000
800
600
400
200
0
0
60m
120m
360m
96h
10d
Time
C
5 mg/L
70 mg/L
Cu2+ mg/L
1
0,5
0
a
b
c
c
96h
10d
Leached Cu 2+ (mg/L)

Figure 2

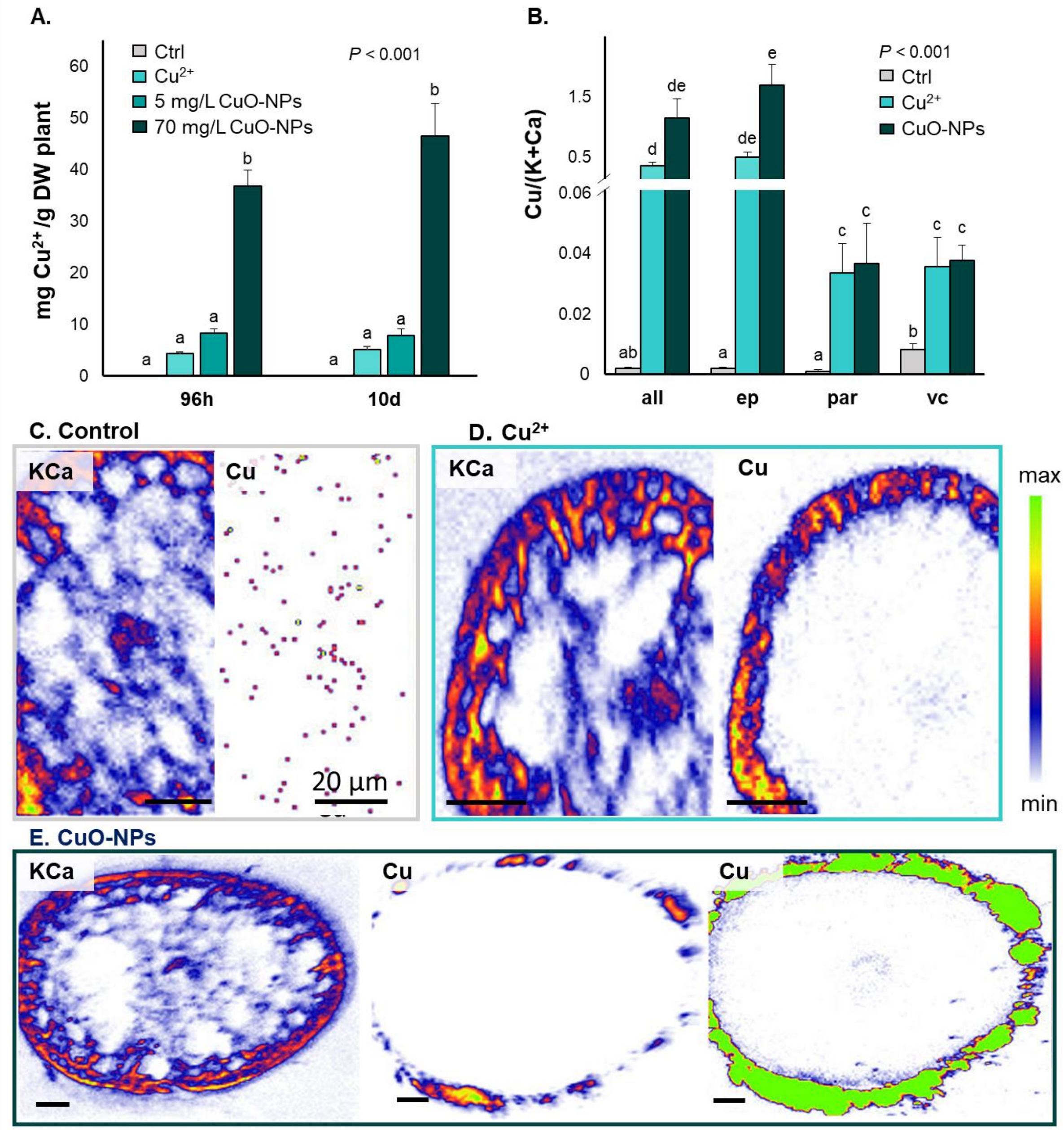

A.
Ctrl
Cu2+
5 mg/L CuO-NPs
70 mg/L CuO-NPs
P < 0.001
mg Cu2+/g DW plant
96h
10d
B.
P < 0.001
Ctrl
Cu2+
CuO-NPs
Cu/(K+Ca)
all
ep
par
vc
C. Control
KCa
Cu
20 µm
D. Cu2+
KCa
Cu
max
min
E. CuO-NPs
KCa
Cu
Cu

Figure 3

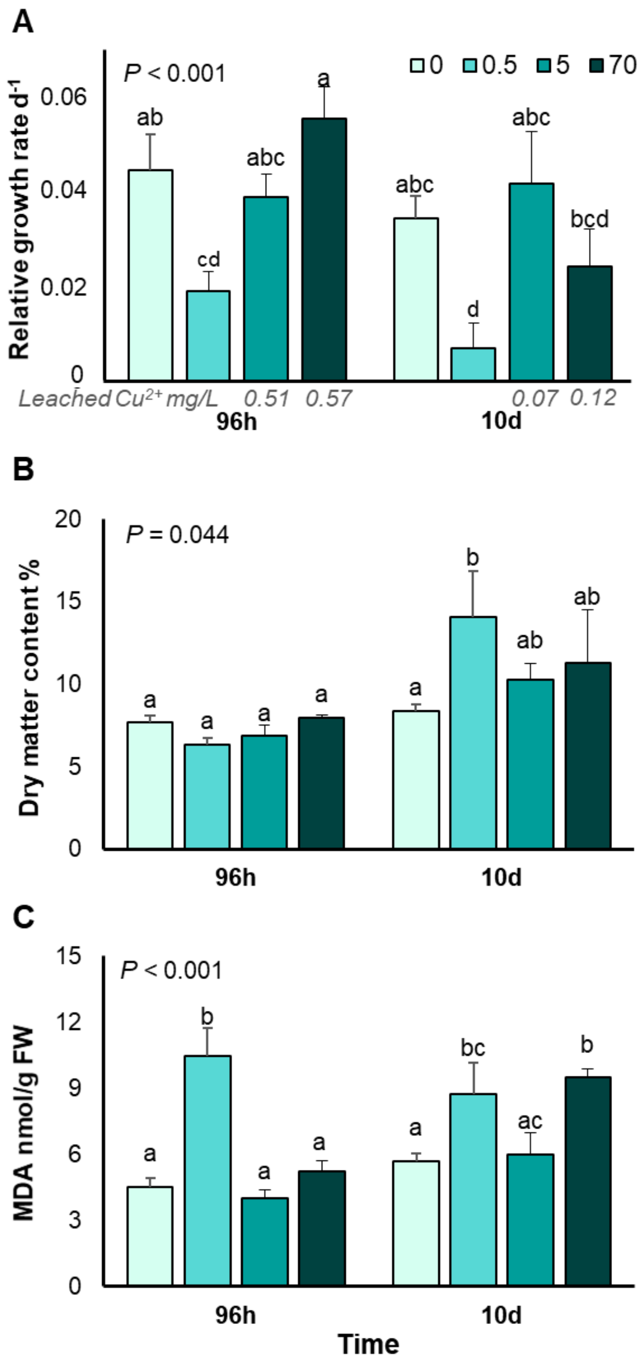
A
P < 0.001
0
0.5
5
70
Relative growth rate d-1
ab
cd
abc
a
abc
d
abc
bcd
Leached Cu2+ mg/L
0.51
0.57
0.07
0.12
96h
10d
B
P = 0.044
Dry matter content %
a
a
a
a
a
b
ab
ab
96h
10d
C
P < 0.001
MDA nmol/g FW
a
b
a
a
a
bc
ac
b
96h
10d
Time

Figure 4

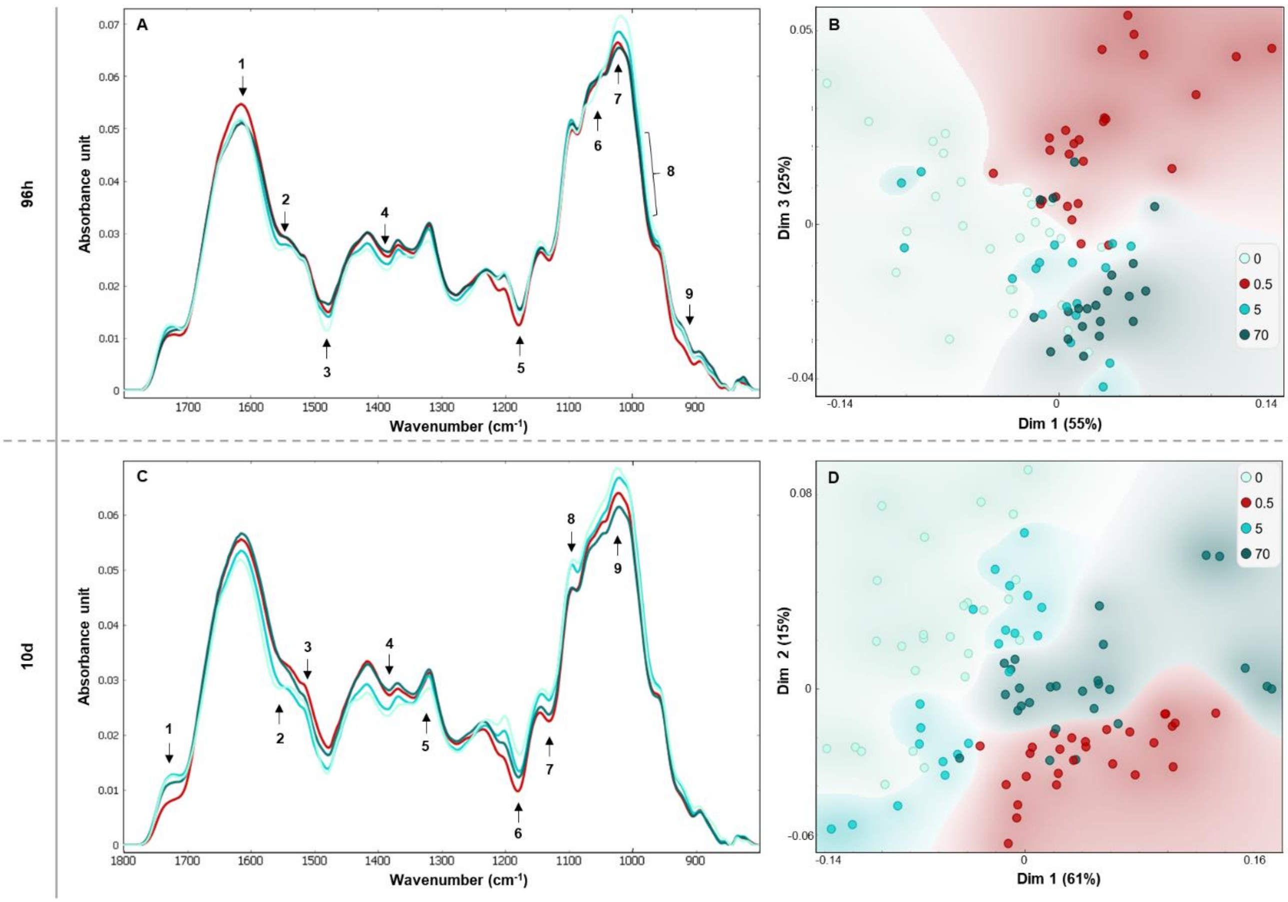

96h
10d
A
B
C
D
Absorbance unit
Wavenumber (cm-1)
Dim 3 (25%)
Dim 1 (55%)
Dim 2 (15%)
Dim 1 (61%)
0
0.5
5
70